Hindawi
Advances in Civil Engineering
Volume 2021, Article ID 9944845, 11 pages
https://doi.org/10.1155/2021/9944845

Research Article

Study on Mechanical Properties of the Expansive Soil Treated with Iron Tailings Sand

Chengfu Chu, Fei Zhang, Daoxiang Wu, Meihuang Zhan, and Yun Liu

Hefei University of Technology, Department of Geotechnical Engineering, School of Resources and Environmental Engineering, Hefei, China

Correspondence should be addressed to Chengfu Chu; chuchengfu@hfut.edu.cn

Received 6 March 2021; Revised 5 April 2021; Accepted 9 April 2021; Published 22 April 2021

Academic Editor: Loke Foong

Aiming at researching shear strength parameters of expansive soil modified by industrial waste iron tailings sand, the enhancement of expansive soil is explored from macroscopic and microscopic aspects. After characterization and testing by various means, the results show that expansive soil modified by iron tailings sand will increase the maximum dry density of the improved soil and reduce its optimal moisture content, which is beneficial in tuning the moisture content at the construction site. In addition, iron tailings sand can improve the shear strength of expansive soils. The influence of iron tailings sand on cohesion increases first, then decreases, and reaches the peak value at 30%, while the effect on internal friction angle exhibits a continuously increasing trend. Furthermore, according to mercury intrusion tests and microangle analysis, the addition of iron tailings sand can reduce the tiny pores and enhance the occlusal force of the soil. Simultaneously, it increases the number of large pores, maximizing the macroscopic strengthening of iron tailings sand towards the expansive soil.

1. Introduction

Iron tailings sand (ITS) is a solid waste discharged from mineral processing and is considered as the main pollution source in the mineral industry. According to relevant statistics, the stacking capacity of ITS in China has exceeded 5 billion tons and is growing with a rate of 500–600 million tons per year [1–3]. The long-term accumulation of ITS takes up abundant land resources and generates serious environmental pollution, which has a seriously detrimental influence on both human beings' health and property safety. However, noting that the main mineral compositions of ITS are SiO_2 and Fe_2O_3 sourced from granite, which has a similar characteristic to the sand usually used in civil engineering projects [4–6], thus, ITS has a high potential to be recycled and applied as the construction material [7–9]. In addition, it can be proved that the iron tailings sand is inclined to inert materials, and the expansive soil improved by iron tailing sand belongs to physical improvement only, does not have the chemical reaction basically, will not produce superfluous chemical pollution, and is greener and safer than other improvement methods [10–13].

Expansive soil is characterized by wetting swelling and drying shrinkage due to changes in water content, which resulted from the high hydrophilic clay minerals, such as montmorillonite and illite [14–17]. This swell-shrinkage characteristic is very likely to cause inhomogeneous deformation of the foundation, further leading to the destruction of the upper constructions [18–20]. Thus, additives such as cement and lime are considered to be added into the expansive soil to weaken the swell-shrinkage characteristic, as well as improving the engineering behavior [21–24]. However, the conventional additives are commonly obtained based on considerable resources consumption, accompanied by the environmental pollution caused by the emission of dust and harmful gases [25, 26]. Therefore, it is a very cost-effective and eco-friendly way to encourage the utilization of recycled solid wastes in the modification of the expansive soils [27, 28]. Numerous research has proved that some industrial by-products, such as fly ash, blast furnace slag, and soda residue, can be recycled for the modification of the problematic soils [29–32] while the study referring to the modification effectiveness of ITS for expansive soil has been rarely reported.

On this basis, this paper investigated the mechanical properties of expansive soil treated with ITS. The free swelling test was performed to evaluate the swelling behavior of the treated soil. Then, the grain distribution analysis test, compaction test, direct shear test, and oedometer test were carried out to study the mechanical properties. Finally, scanning microscopy electron test (SEM) and mercury intrusion porosimetry (MIP) test were conducted on the treated soil to reveal the modification mechanisms of the ITS treated expansive soil [33–36].

2. Materials and Methods

2.1. Materials. The tested soil was sampled in a foundation pit, which was located in the northeast corner of Tunxi Road Campus of Hefei University of Technology, at depth of 3.4~3.8 meters, containing calcium or iron-manganese concretion. The basic physical properties of the natural soil are presented in Table 1, while the predominant mineral compositions were identified by X-ray diffraction (XRD) as shown in Figure 1. As presented in Table 1, the free swelling rate of natural soil is 52.5%. According to the previous research [37–39], the tested soil can be classified as weakly expansive soil.

Iron tailings sand (ITS) used in the paper was taken from an iron ore mine in Lujiang County, Anhui Province. The main chemical compositions tested by X-ray fluorescence spectrometry (XRF) are listed in Table 2. ITS is predominantly composed of SiO_2, Fe_2O_3, Al_2O_3, and a little MgO and CaO.

Figure 2 shows the grain fraction curve of expansive soil and ITS. According to the size of the sample, the expansive soil was tested by a laser particle size analyzer, and the iron tailing sand was tested by the sieving method. It can be seen from the figure that the particle size of expansive soil is relatively small and the distribution range is mainly 2–10 μm, while the particle size of ITS is relatively large, mainly 100–1000 μm [40–43].

2.2. Sample Preparation. The tested soil and ITS were dried in an oven at 105°C for 24 h and then pulverized, passing through a 2 mm sieve. Mixing soil with ITS thoroughly, the mass ratio of ITS to soil was controlled at 0%, 10%, 20%, 30%, 40%, and 50%. A certain quantity of distilled water was poured into the sand-soil mixture and stirred evenly. Subsequently, the mixture was sealed in the plastic bag for 24 h, subsequently to prepare the cut ring sample with dimensions of Φ61.8 mm × H20.0 mm by the static compaction method [44, 45].

2.3. Methods

2.3.1. Grain Distribution Analysis Test. For the plain soil samples, the laser particle size analyzer was used directly without further screening. For the soil samples with different ITS content, a combination of the sifting method and laser particle size analysis method was adopted. The soil samples with a particle size greater than 0.075 mm were tested by the sifting method, while the soil samples with a particle size less than 0.075 mm were tested by a laser particle size analyzer. MS-2000 laser particle size analyzer was used in the laser particle size analysis test.

2.3.2. Compaction Test. After the sample preparation (sample sieved with a 5 mm sieve), dry samples were prepared according to the test standard (GB/T5012-1999) [46, 47] and tested to measure the dry density and moisture content of each group of samples, respectively. Finally, the optimal moisture content and maximum dry density were obtained after finishing.

2.3.3. Free Swelling Test. After sample preparation (sample sieved with a 0.5 mm sieve), the sample was prepared according to the test standard (GB/T5012-1999) and tested. When the data was finally recorded, the readings were recorded every 2h until the difference between the two readings was less than 0.2 ml. The test could be completed.

2.3.4. Direct Shear Test. After sample preparation, the sample was prepared according to the test standard (GB/T5012-1999) and tested. Zj-2 strain-controlled direct shear apparatus is used to carry out the nonconsolidation and nondrainage direct shear test on soil samples. The vertical pressure of the sample of the modified expansive soil with single ITS is set as 50, 100, 200, 300, and 400 kPa, and the shear rate is 0.8 mm/min. The loss is reduced within 3–5 min. The dial indicator reading is recorded every turn until the shear loss.

2.3.5. Oedometer Test. After sample preparation, the sample was prepared according to the test standard (GB/T5012-1999) and tested. The pressure classes used in this test are 12.5, 25, 50, 100, 200, 400, 800, and 1600 kPa, which are automatically recorded by the computer according to the standard time [48–50].

2.3.6. Scanning Microscopy Electron Test (SEM). The sample preparation method is the same as that of consolidation test, which is to make Φ61.8 mm × H20 mm ring knife sample, then put the sample into the standard curing box, and take it out for test after reaching the fixed curing age. Firstly, the soil sample was cut into a cuboid with dimensions of 5 mm × 5 mm × 10 mm and freeze-dried for 24 h. After that, the sample was divided carefully into two pieces by hand. The relatively flat and thin clay was selected as the tested sample, and the fracture surface was set as the observation plane. Finally, the tested sample was sprayed with gold by vacuum coating apparatus, followed by the morphology observation. In the process of sample breaking, attention should be paid to keep the fresh section of the soil sample from being collided and let alone being contaminated by contact with other substances.

Table 1: Basic physical properties of expansive soil.

Water content (%)	Specific gravity	Void ratio	Liquid limit (%)	Plastic limit (%)	Cohesion (kPa)	Internal friction angle (°)	Free swelling index (%)
25.7	2.68	0.74	45.5	22.3	74.3	27.6	52.5

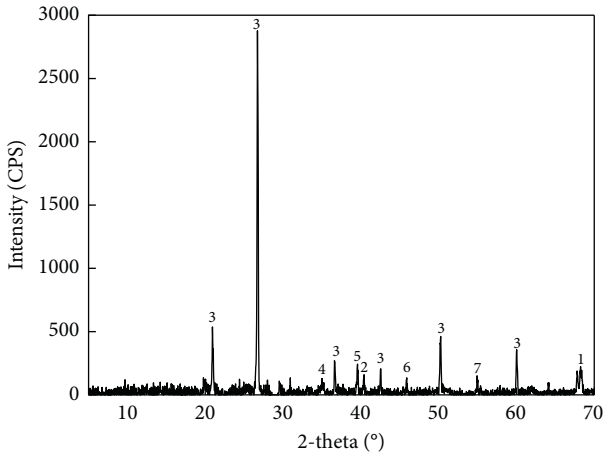

Figure 1: Mineral compositions of the tested soil.

Table 2: Main chemical components of ITS.

Chemical composition	SiO_2	Al_2O_3	Fe_2O_3	CaO	MgO	SO_3
Content (%)	63.21	8.91	12.53	4.08	6.25	5.02

2.3.7. Mercury Intrusion Porosimetry (MIP). The preliminary sample preparation of the mercury injection test is consistent with the scanning electron microscope test; that is, the soil sample was cut into a cuboid with dimensions of 10 mm × 10 mm × 10 mm and freeze-dried for 24 h. The mercury injection instrument used in the test is AutoPore9500 automatic mercury injection instrument, and the pressure range is 0.1 to 60000 psia. The mercury injection test uses the property that noninvasive liquids do not flow into solid pores in the absence of pressure. According to the formula, the pore size can be calculated according to different pressures. Then, the relation curve between the cumulative mercury intake and the pore diameter can be drawn according to the mercury intake corresponding to different pore diameters to calculate the percentage of pores of different sizes in the total, in order to understand the distribution of different pores in soil [51–53].

3. Results and Discussion

3.1. Gradation Curve. The particle size distribution range of the expansive soil treated by iron tailings sand (ITS) with various contents is shown in Figure 3 and the uniformity coefficient of the ITS treated expansive soil is shown in Figure 4.

From the results of the experiment, we can see that, with the increase of ITS, the grain size curve of soil samples gradually becomes flat, and the uniformity coefficient (Cu) also gradually increases. Moreover, when the ITS content reached 30%, the grain size of the soil sample was not uniform, and the grain grading was significantly improved compared with the low ITS content sample so that the strength and compactness of the improved soil were increased, and the compressibility of the soil was reduced, which was just mutually verified with the results of the consolidation test [54].

3.2. Compaction Characteristic. The compaction curves of the expansive soil treated by iron tailings sand (ITS) with various contents are shown in Figure 5.

As illustrated in Figure 5, increasing the ITS content leads to an obvious growth in the maximum dry density, as well as a significant reduction in the optimum moisture content. The addition of ITS into expansive soil causes an increase in the specific gravity, which results in the growth of the maximum dry density. Besides, ITS is almost inactive, hydrophobic, and nonhydraulic [55, 56]. When the hydrophilic soil particles are partially replaced by the hydrophobic ITS, the hydrophily of the expansive soil is weakened. Thus, the optimum moisture content is reduced.

3.3. Free Swelling Index. The effects of ITS content on the free swelling index of the treated samples are illustrated in Figure 6.

As shown in Figure 6, the free swelling index decreases significantly with ITS content increasing. It can be observed that the free swelling index is lower than 40% as soon as the ITS content increases up to 20%. It is suggested that the swelling properties of the expansive soil can be effectively modified to satisfy the requirement of the engineering practice by mixing with ITS. The improvement of expansive soil of ITS is mainly to replace part of the soil into ITS without swelling by displacement. With the increase of ITS content, the isolated sand particles gradually transformed to connected sand skeleton. Consequently, the swelling potential of clay particles was restricted by the sand skeleton, leading to an obvious reduction of the free swelling index.

Besides, it can be seen from Figure 6 that the decreasing rate of the free swelling index appears to be slightly lower as the ITS content exceeds 30%. It is because ITS is an inert substance that just induces a physical modification of the expansive soil, accounting for the failure to continuously reduce the swelling behavior of the specimens.

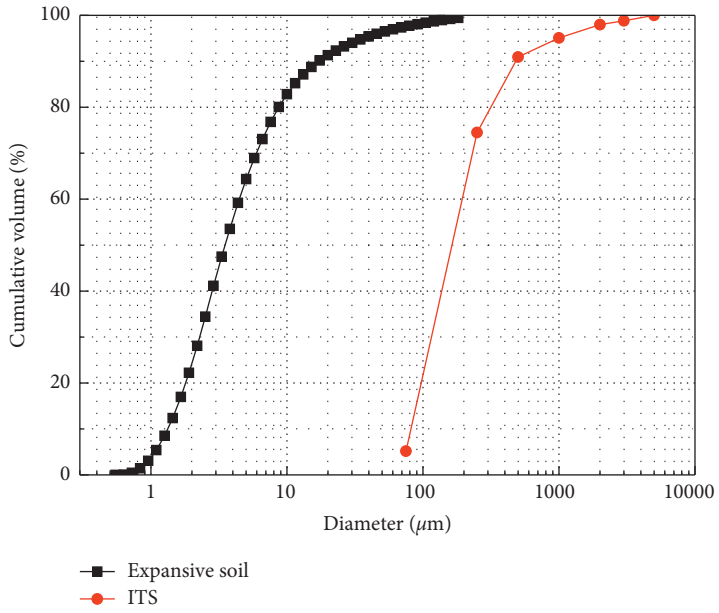

Figure 2: Particle size distribution range of expansive soil and ITS.

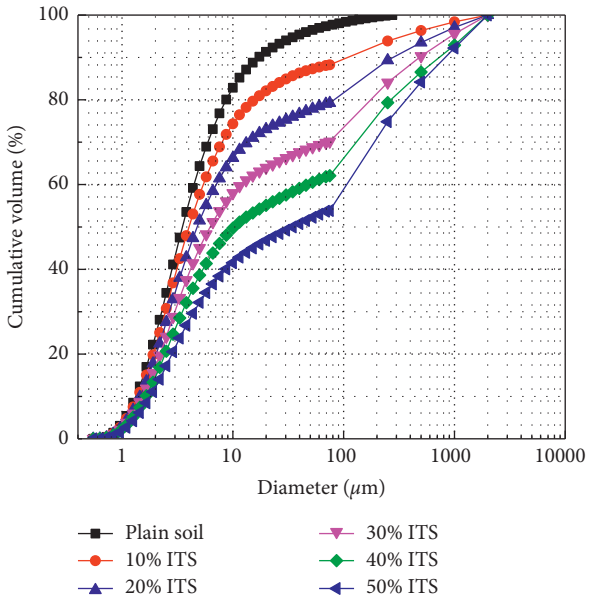

Figure 3: Particle size distribution range of the ITS treated expansive soil.

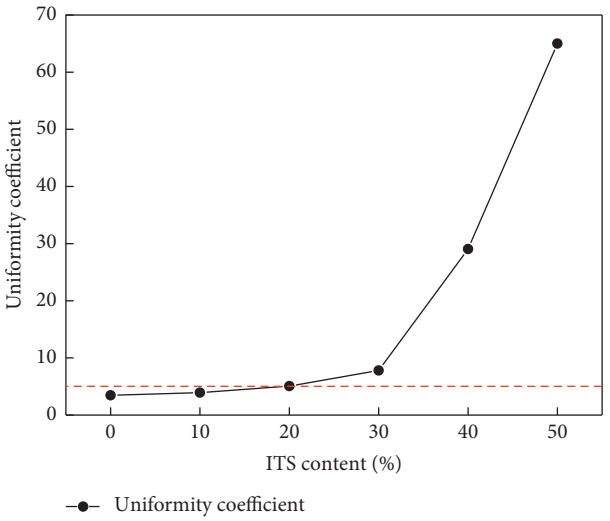

Figure 4: Uniformity coefficient of the ITS treated expansive soil.

3.4. Shear Strength. Figure 7 presents the variations of the cohesion and internal friction angle of the treated specimens with different ITS contents. As can be seen from Figure 7, the incorporation of ITS can enhance the cohesion and internal friction angle of the expansive soil effectively. The internal friction angle increases apparently with ITS content increasing. The increment of the cohesion appears to be slight, and the increasing tendency terminates at ITS content of 30%. It indicates that the addition of ITS within a certain range of quantity has a reinforcing effect on the cohesion of the expansive soil within a certain range. While the sequential addition of ITS will impose a detrimental impact on the shearing strength of the treated specimens.

As aforementioned, the modification of expansive soil with ITS is a pure physical process, so the ITS itself has little influence on the cohesion of the specimens. The modified soil is composed of the continuous medium (soil particles) and discontinuous medium (ITS). In the shear test, with the increase of sand-mixing rate, the grain gradation of modified soil was improved, which enhanced the original cohesive force of soil to some extent. However, the connection between the ITS particles and expansive soil particles is still less tight than that of the soil particles themselves, and there are still slightly larger gaps in the solidification process than that of the original soil, so the solidification adhesion and capillary adhesion of the soil are somewhat reduced. Therefore,

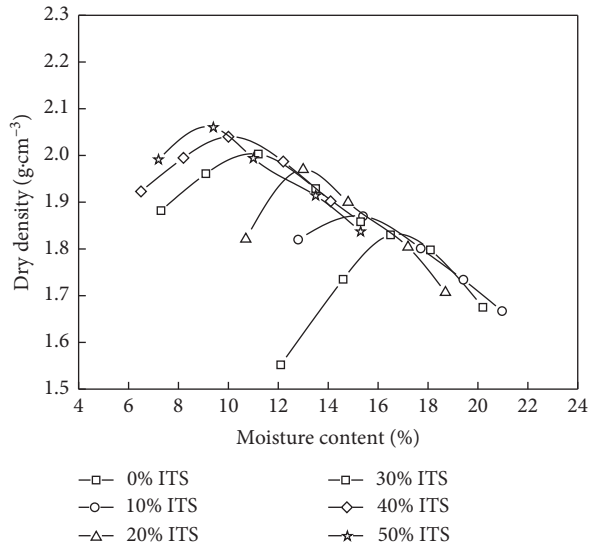

Figure 5: Compaction curves of the ITS treated expansive soil.

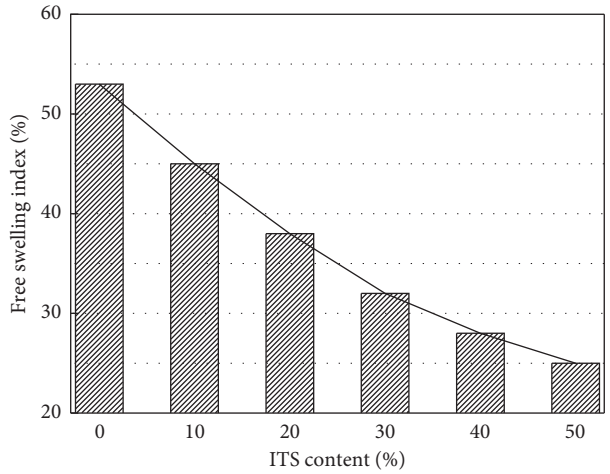

Figure 6: Relationship between the swelling index and ITS content.

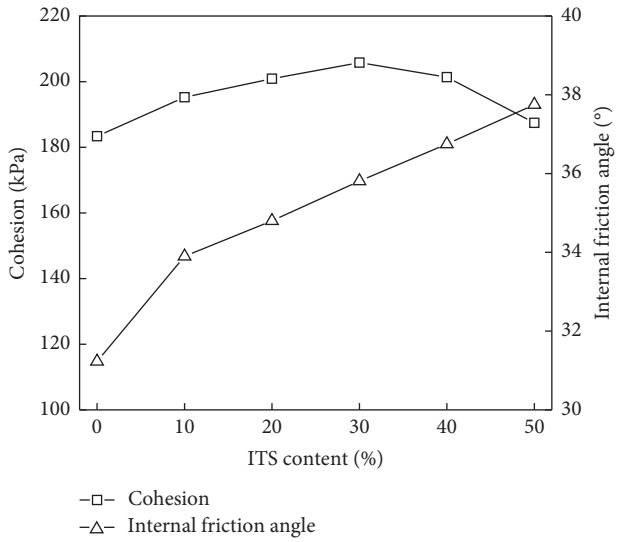

Figure 7: Variations of the cohesion and internal friction angle with ITS content.

the original cohesive force of the soil increases rapidly under a low sand-mixing rate, and the cohesive force increases slowly on the whole. However, when the sand-mixing rate exceeds a certain threshold, the cohesive force of the three kinds of soil decreases to different degrees, and the cohesive force decreases gradually on the whole.

The internal friction angle of the soil is determined by the mutual sliding friction and interlocking action between soil particles [57–59]. The addition of ITS into expansive soil can strongly enhance the interlocking action between soil particles, meanwhile increasing the slide friction.

Figure 8 presents the relationships between the shear strength of the treated soil and ITS content. The shear strength increases first as the ITS content varies from 0 to 40%, and then decreases as the ITS content increases up to 50%. With respect to the shear strength, there is a threshold content for the modification of expansive soil based on ITS.

3.5. Compressibility. The e-log (p) curves of the ITS treated specimens with different contents are obtained by the Oedometer test, as shown in Figure 9.

At low vertical stress, the sample is compressed by discharging partial water and gas from the pores of the soil, which is characterized by elastic deformation. When the vertical stress increases up to a certain value, plastic deformation gradually occurs. In addition, the yield point gradually appears to be less obvious as the ITS content increases. It is suggested that the addition of ITS is available for improving the capacity against compressive deformation induced by the excessive overburden.

Figure 10 shows the variations of compression modulus with increasing ITS content. It can be seen that the compression modulus increases significantly with ITS increasing. On this basis, it can be concluded that adding ITS into expansive soil can effectively reduce its compressibility.

3.6. Microstructural Characteristics

3.6.1. SEM. In order to reveal the modification mechanisms of ITS treated expansive soil, the micromorphology of the specimens was determined by SEM technology, as shown in Figure 11.

The incorporation of ITS has little effect on the earthiness of expansive soil. As mentioned above, the addition of ITS has a positive promoting effect on the shear strength of the expansive soil. In addition, it can be seen that the binding effect between iron tailings sand particles and soil particles is not invariable with the change of sand-mixing rate. As can be seen from Figure 11, both undisturbed soil and modified soil have a certain number of pores, most of which have a width of 1–20 μm. With the increase of sand-mixing rate, the pore size between the ITS particles and the soil particles in the modified soil does not change significantly, but only the pore number changes. At the interval of 0%~20% sand-mixing rate, with the increase of sand-mixing rate, the medium and small pores in the sample (see the law of pore division for details in the mercury injection experiment) also gradually increased. When the proportion of sand-mixing

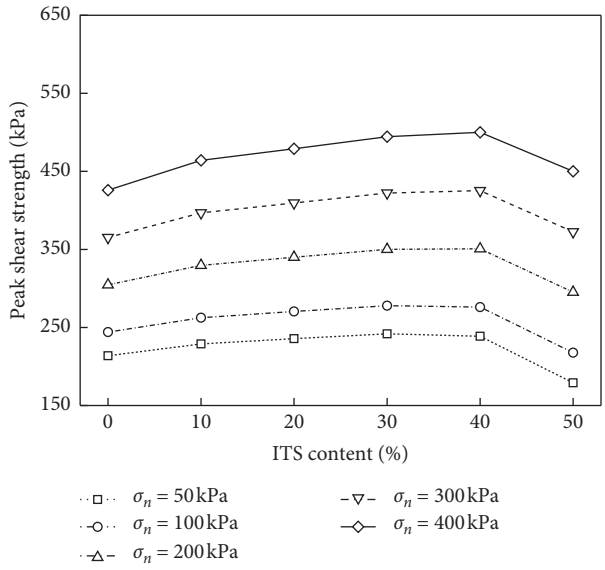

Figure 8: Variations of the peak shear strength with ITS content.

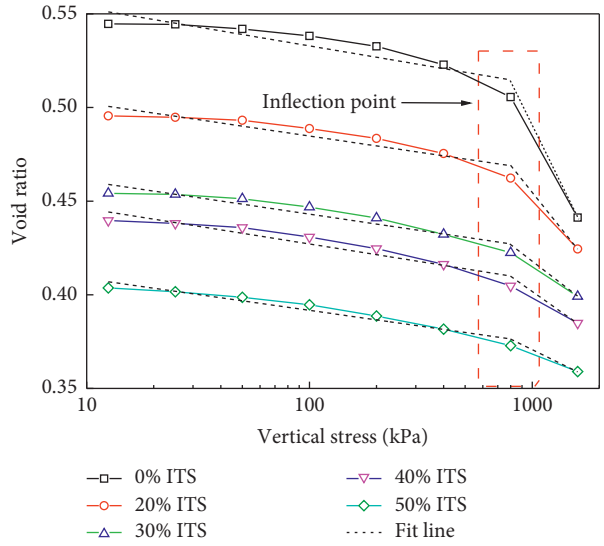

Figure 9: e-log (p) curves of the ITS treated specimens with different contents.

rate is 30%, the degree of connection between ITS and soil particles is the best, and the porosity is small and evenly distributed. When the sand-mixing rate exceeds 30%, the pore quantity increases accordingly.

Combined with the SEM images and pore distribution rules of soil samples, it cannot only prove the changing rules of the shear strength parameters of the modified soil samples; that is, under the actual pressure, the ITS of the samples with 30% sand-mixing rate is most closely bound to the soil particles and have the highest shear strength. In addition, it can also be shown that the free swelling index of the sample decreases with the increase of the sand-mixing rate. This is mainly because, under the low sand-mixing rate, the SEM image shows that the ITS particles are less and far from each other, and the pores between sand and soil particles are

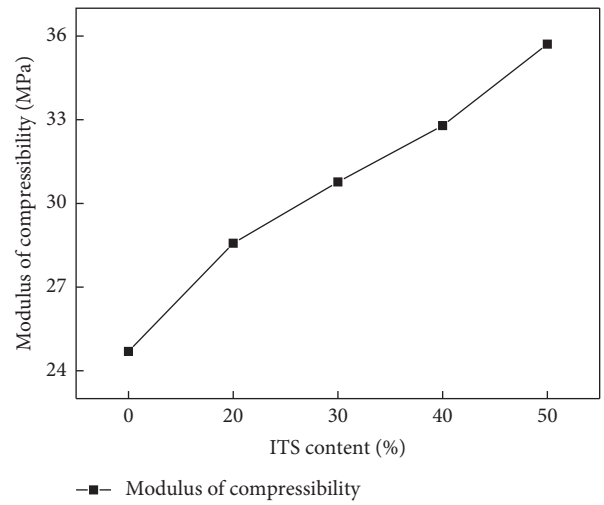

Figure 10: Variations of the compression parameters with ITS content.

relatively large, so the free swelling index of the sample is relatively high. With the increase of sand-mixing rate, the particles of ITS gradually increase and get closer to each other. Under the 30% sand-mixing rate, the optimal value of ITS and soil particles can be reached, and the porosity and the free swelling index can be reduced.

And under the high sand-mixing rate, the ITS displace a large number of soil particles, while making sample grading improve. However, the ITS and soil particles basically do not react chemically, the pores between ITS and soil particles increase, and more sand particles are close to each other and form a sand skeleton, which further restricts the expansiveness of expansive soil so that the free swelling index of the sample is further reduced, but the falling range is significantly reduced.

3.6.2. Pore Size Distribution. In order to investigate the effect of the addition of ITS on the characterization of the pore size distribution of the expansive soil, the MIP test was performed, and the results are presented in Figures 12 and 13.

Referring to Shear's [60] criteria, soil pores can be classified as five types, including micropores ($d < 0.007\,\mu$m), small pores ($0.007\,\mu\text{m} < d < 0.9\,\mu$m), mesopores ($0.9\,\mu\text{m} < d < 35\,\mu$m), and macropores ($35\,\mu\text{m} < d < 2000\,\mu$m). These pores are defined as pore within the soil particles, intergranular pore, intra-aggregate pore, and interaggregate pore, respectively. Note that those pores of more than 300 μm can be defined as macroscopic pores.

The variation of cumulative pore volume with aperture was depicted in Figure 12. And the specific process can be roughly divided into the following three stages.

The first stage of infiltration is dominated by pores with a radius of 5~300 μm, including the macropores and partial mesopores affected by the sand-mixing rate. The curves of cumulative pore volume vary with the sand-mixing rate. On the whole, due to the incorporation of ITS with a larger particle size than soil particles, the modified soil particle size was improved

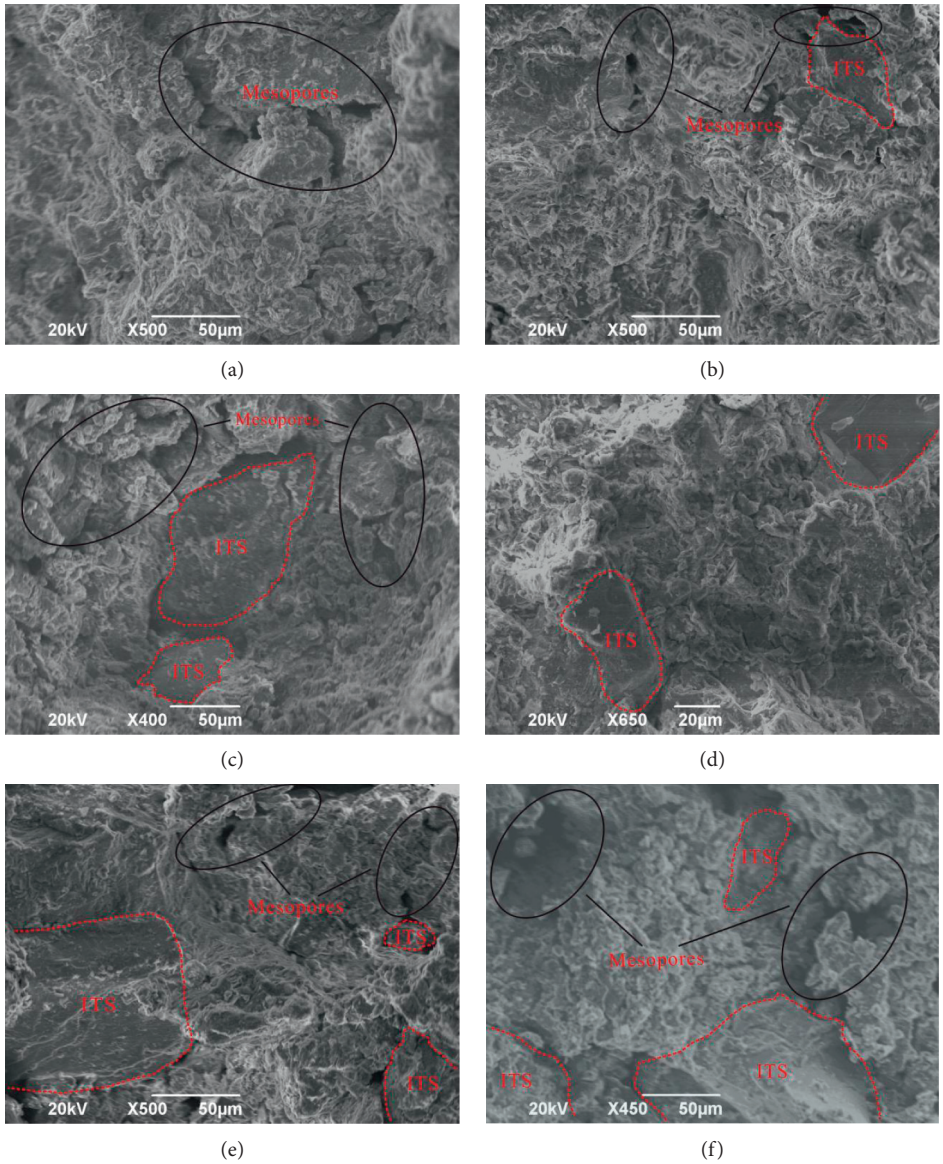

Figure 11: Microstructure of the soil samples before and after modification. (a) Natural soil. (b) 10% ITS. (c) 20% ITS. (d) 30% ITS. (e) 40% ITS. (f) 50% ITS.

to some extent. However, according to the corresponding SEM images, the connection between ITS particles and soil particles was not very good, and there were more mesopores in this interval than plain soil. It can be seen from Figure 12 that the sample with a sand-mixing rate of 30% has the smallest number of pores in all the modified soils (excluding plain soil), which is consistent with the SEM image results.

The second stage of infiltration mainly involves pores with a radius of 0.2~5 μm, containing the residual mesopores and partial small pores. The curves of cumulative pore volume are nearly the same under different sand-mixing rates, signifying that the pores at this stage are unacted on the sand-mixing rate.

The third stage of infiltration is basically aimed at pores with a radius of 0.005~0.2 μm, covering micropores and the remaining small pores. The cumulative pore volume decreases gradually accompanied by the increasing sand-mixing rate, which can be explained as follows: the ITS has a large particle size without forming small pores and micropores. This property determines that the pore change at this stage arises from the incorporation of ITS to replace the soil. The soil is a three-phase system with internal pores, while the ITS is a solid phase with a few internal pores. Therefore, replacing expansive soil with ITS is equivalent to replacing the porous three-phase system with a nonporous solid phase, which undoubtably decreases the micropores and small pores inside the improved soil.

Figure 13 shows the pore size distribution of the treated soil with different ITS content. The pore size distribution diagram of the modified soil has a distinct three-peak structure. The first peak is situated between 0.005 and 0.05 μm, belonging to microporous and partial small pores. And the second peak lies between 0.2 and 3 μm, defining as small pores and partial mesopores, and has a sharp peak at

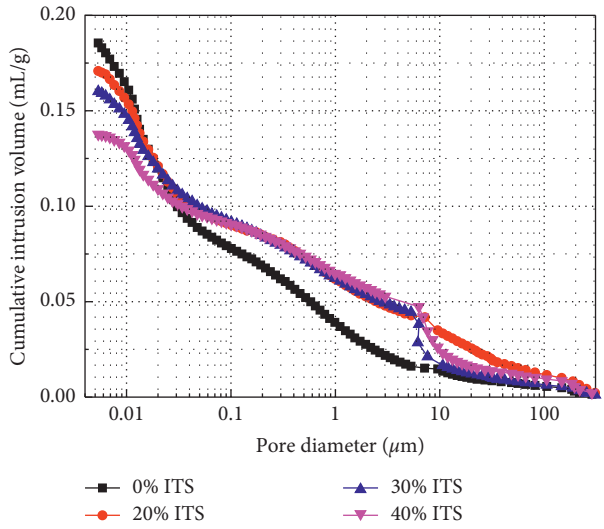

Figure 12: Relationship between cumulative pore volume and aperture.

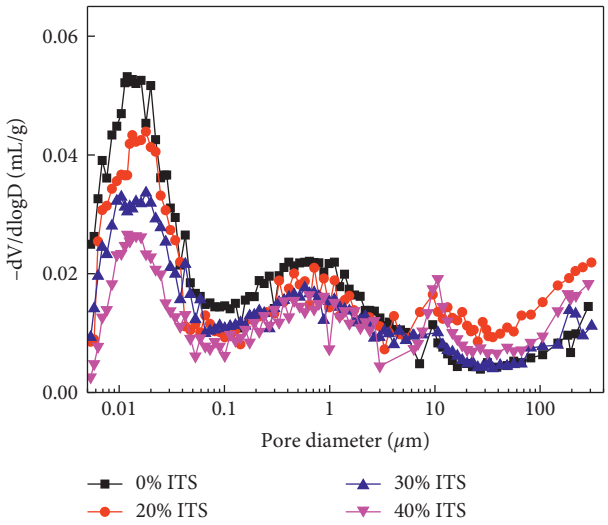

Figure 13: Relationship between the incremental saturation of mercury and the aperture.

about 0.7 μm. The third peak lies between 5 and 11 μm, belonging to mesopores. Thus, it is concluded that the pores of the modified soil are mainly composed of two parts: one is the intrinsic micropores and small pores of the soil particles, and the other is the mesopores generated by the incorporation of ITS. In addition, the plain soil has a bimodal structure, and compared with the modified soil, only the mesopores formed after the addition of ITS are missing.

In fact, corresponding to the pressure of about 207 kPa and the aperture of about 7 μm, the sample is in the high- and low-pressure conversion of the mercury porosimeter, so there are fewer data points collected at this time, which will not affect the cumulative amount of mercury. But it will cause the saturation of mercury increment to be higher, so the data at this point in this article has been

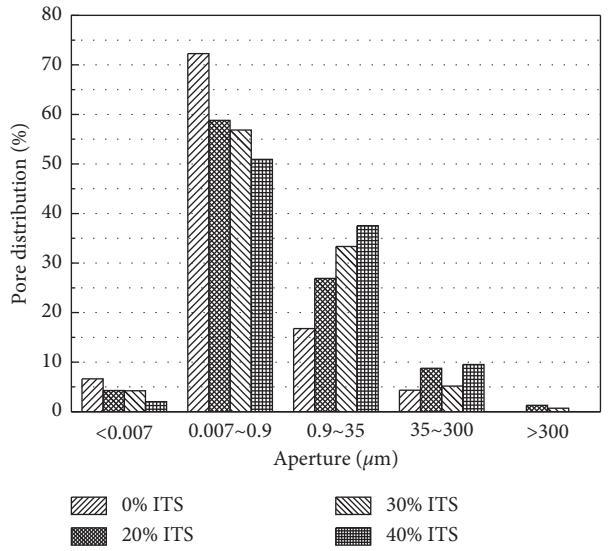

Figure 14: Relationship between the percentage of different pore distribution and aperture.

corrected by the author to ensure the accuracy of the experimental data.

As we can see from Figure 14, the pores of plain soil are dominated by small pores of 0.007~0.9 μm, up to 72%, and the small pores and mesopores account for about 90% of the total pores. With the ITS mixed, the pores still concentrate on small pores and mesopores, whose contents are all above 85%. The difference is that as the sand-mixing rate increases, the average aperture is increasing. The incorporation of ITS reduces the proportion of micropores and small pores in the soil while increasing the proportion of macropores and mesopores. In particular, the percentage of macropores in the soil reaches the lowest with the sand-mixing rate of 30%, representing the optimal adhesion between the agglomerates. The conclusion confirms again the consistency of macro- and microtesting results.

4. Conclusions

In this paper, the industrial waste ITS is employed to modify the expansive soil. After characterization and testing by various techniques, the following conclusions are drawn.

(1) Modifying expansive soil by ITS enlarges the maximum dry density of the improved soil and reduces its optimal moisture content. The compaction curve is gentler with the rising of the sand-mixing ratio, which is conducive to controlling the moisture content at the construction site. And when the sand-mixing ratio exceeds 20%, the modified soil can be regarded as nonexpansive soil.

(2) The ITS can improve the shear strength of the expansive soil. The effect on the cohesion is firstly increased and then decreased. When the ITS content is 30%, the shear strength reaches a peak value, and the effect on the internal friction angle is continuously increased. The formed sand-clay mixture has

improved properties in compressive properties. The ITS in the soil can effectively resist the compression deformation caused by the load, thereby improving the compressive capacity of the expansive soil.

(3) The SEM images show that ITS is unacted on the microstructure of expansive soil except for the crack around 10 μm between sand and soil. Sand particles simultaneously improve the biting force and the porosity in the soil, indicating that there exists a threshold content for ITS to realize the maximum macroscopic strength of the expansive soil. The mercury injection test reveals that the incorporation of ITS reduces the proportion of the micropores and small pores in the soil, leading to a larger average aperture. The pore size distribution diagram of modified soil has a distinct bimodal structure, which explains macroscopical mechanical laws nicely.

In conclusion, the use of ITS to improve expansive soil not only solves the problem of environmental pollution caused by waste ITS but also saves the use of cement and lime on the basis of improving the soil quality of the project and reduces the project cost. And through the test, we know that when the sand-mixing rate is 30%, it is the best improvement effect.

Data Availability

All the data in this paper are obtained by the author's independent laboratory test, which can ensure the authenticity and reliability of the test data.

Conflicts of Interest

On behalf of all authors, the corresponding author states that there are no conflicts of interest.

Acknowledgments

The authors are grateful for the financial support of the Anhui Provincial National Science Foundation (Grant no. 2008085MD118) and the National Science Foundation of China (Grant no. 41572280).

References

[1] J. Liu, Y. Liu, and X. Wang, "An environmental assessment model of construction and demolition waste based on system dynamics: a case study in Guangzhou," *Environmental Science and Pollution Research*, vol. 27, no. 30, pp. 37237–37259, 2020.

[2] B. Mou, X. Li, Y. Bai, and L. Wang, "Shear behavior of panel zones in steel beam-to-column connections with unequal depth of outer annular stiffener," *Journal of Structural Engineering*, vol. 145, no. 2, pp. 4018247–4018264, 2019.

[3] J. Liu, Y. Yi, and X. Wang, "Exploring factors influencing construction waste reduction: a structural equation modeling approach," *Journal of Cleaner Production*, vol. 276, pp. 123185–123201, 2020.

[4] Y. Tai, J. Wang, W. Chen et al., "A BIM-based approach for predicting corrosion under insulation," *Automation in Construction*, vol. 107, pp. 102923–102941, 2019.

[5] C. Liu, F. Wang, L. He, X. Deng, J. Liu, and Y. Wu, "Experimental and numerical investigation on dynamic responses of the umbrella membrane structure excited by heavy rainfall," *Journal of Vibration and Control*, vol. 27, no. 5-6, pp. 675–684, 2020.

[6] C. Liu, F. Wang, X. Deng et al., "Hailstone-induced dynamic responses of pretensioned umbrella membrane structure," *Advances in Structural Engineering*, vol. 24, no. 1, pp. 3–16, 2021.

[7] Y. Wang, A. Wu, and L. Zhang, "Investigation of the sedimentation property of backfill material on the basis of rheological test: a case study of iron tailings," *Journal of Chemistry*, vol. 2018, Article ID 9530767, 9 pages, 2018.

[8] A. U. Shettima, M. W. Hussin, Y. Ahmad, and J. Mirza, "Evaluation of iron ore tailings as replacement for fine aggregate in concrete," *Construction and Building Materials*, vol. 120, pp. 72–79, 2016.

[9] E. Lakovleva, P. Maydannik, and V. Tatiana, "lvanova. Modified and unmodified low-cost iron-containing solid wastes as adsorbents for efficient removal of As(III) and As(V) from mine water," *Journal of Cleaner Production*, vol. 133, pp. 1095–1104, 2016.

[10] H. Huang, M. Huang, W. Zhang, S. Pospisil, and T. Wu, "Experimental investigation on rehabilitation of corroded RC columns with BSP and HPFL under combined loadings," *Journal of Structural Engineering*, vol. 146, no. 8, pp. 4020157–4020175, 2020.

[11] X. Li, Y. Feng, B. Liu et al., "Influence of NbC particles on microstructure and mechanical properties of AlCoCrFeNi high-entropy alloy coatings prepared by laser cladding," *Journal of Alloys and Compounds*, vol. 788, pp. 485–494, 2019.

[12] Y. Ju, T. Shen, and D. Wang, "Bonding behavior between reactive powder concrete and normal strength concrete," *Construction and Building Materials*, vol. 242, pp. 118024–118033, 2020.

[13] C. Zhang, G. Gholamreza Mousavi, and A. Alsadat, "State-of-the-art review on responses of RC structures subjected to lateral impact loads," *Archives of Computational Methods in Engineering*, 2020.

[14] I. Shenglin, S. Qin, Z. Bao, and B. Shi, *Research on Engineering Geology of Expansive Soil in China*, Vol. 67, Jiangsu Science and Technology Press, Nanjing, China, 1992.

[15] X. Zhu, Z. Cai, and Y. Huang, "Research on mechanical properties and damage evolution law of expensive soils under the cyclic action of coupling wetting-drying and freeze-thaw," *Chinese Journal of Rock Mechanics and Engineering*, vol. 6, pp. 1233–1241, 2019.

[16] P. M. Amarasinghe, K. S. Katti, and D. R. Katti, "Insight into role of clay-fluid molecular interactions on permeability and consolidation behavior of na-montmorillonite swelling clay," *Journal of Geotechnical and Geoenvironmental Engineering*, vol. 138, no. 2, pp. 138–146, 2012.

[17] S. Amin, A. Deng, and A. Taheri, "Swell–compression characteristics of a fiber–reinforced expansive soil," *Geotextiles and Geomembranes*, vol. 46, no. 2, pp. 183–189, 2018.

[18] J. Zhang, P. He, J. Xiao, and F. Xu, "Risk assessment model of expansive soil slope stability based on Fuzzy-AHP method and its engineering application," *Geomatics, Natural Hazards and Risk*, vol. 9, no. 1, pp. 389–402, 2018.

[19] W. Li, G. Liu, W. Wang et al., "Study on the crack propagation law of compacted expansive soil under wet-drying cycle," *Geotechnical Engineering*, vol. 36, no. 7, pp. 1302–1308, 2014.

[20] W. Hamid, L. Samang, and T. Harianto, "Geotechnical profiles of expansive soil hazard for road infrastructure: case

study of Takalar-Jeneponto provincial road corridor," *IOP Conference Series: Earth and Environmental Science*, vol. 419, 2020.

[21] S. Bhuvaneshwari, R. G. Robinson, and S. R. Gandhi, "Resilient modulus of lime treated expansive soil," *Geotechnical and Geological Engineering*, vol. 37, no. 1, pp. 305–315, 2019.

[22] P. Indiramma, C. Sudharani, and S. Needhidasan, "Utilization of fly ash and lime to stabilize the expansive soil and to sustain pollution free environment - an experimental study," *Materials Today: Proceedings*, vol. 22, no. 3, pp. 694–700, 2020.

[23] V. Panich and J. Pitthaya, "Characteristics of expansive soils improved with cement and fly ash in Northern Thailand," *Geomechanics and Engineering*, vol. 6, no. 5, pp. 437–453, 2016.

[24] Y. Lu, S. Liu, and Y. Zhang, "Freeze-thaw performance of a cement-treated expansive soil," *Cold Regions Science and Technology*, vol. 170, Article ID 102926, 2020.

[25] D. Song, J. Yang, B. Chen, T. Hayat, and A. Alsaedi, "Life-cycle environmental impact analysis of a typical cement production chain," *Applied Energy*, vol. 164, pp. 916–923, 2016.

[26] M. Naeimi and A. Haddad, "Environmental impacts of chemical and microbial grouting," *Environmental Science and Pollution Research*, vol. 27, no. 2, pp. 2264–2272, 2020.

[27] Z. Alam, C. Zhang, and S. Bijan, "Influence of seismic incident angle on response uncertainty and structural performance of tall asymmetric structure," *The Structural Design of Tall and Special Buildings*, vol. 29, no. 12, 2020.

[28] C. Li, Li Sun, Z. Xu et al., "Experimental investigation and error analysis of high precision FBG displacement sensor for structural health monitoring," *International Journal of Structural Stability and Dynamics*, vol. 20, no. 6, 2020.

[29] H. Zhao, C. Chu, K. Guo, and H. Ye, "Experimental analysis of the basic engineering properties of expansive soils improved by iron tailings sand," *Architectural & Environmental Engineering*, vol. 39, no. 6, pp. 98–104, 2017.

[30] X. Zhuang, Z. Wang, and W. Yang, "Experimental study on strength characteristics of expansive soil improved by fly ash-natural sand," *Yangtze River Academy*, vol. 36, no. 8, pp. 86–89, 2019.

[31] R. A. Blayi, A. F. H. Sherwani, H. H. Ibrahim et al., "Strength improvement of expansive soil by utilizing waste glass powder," *Case Studies in Construction Materials*, vol. 13, Article ID e00427, 2020.

[32] S. Akbulut and A. Saglamer, "Modification of hydraulic conductivity in granular soils using waste materials," *Waste Management*, vol. 24, no. 5, pp. 491–499, 2004.

[33] C. Zhang and H. Wang, "Swing vibration control of suspended structure using active rotary inertia driver system: parametric analysis and experimental verification," *Applied Sciences*, vol. 9, no. 15, 2019.

[34] C. Zhang, Z. Alam, Li Sun et al., "Fibre Bragg grating sensor-based damage response monitoring of an asymmetric reinforced concrete shear wall structure subjected to progressive seismic loads," *Structural Control and Health Monitoring*, vol. 26, no. 3, pp. 2307–2331, 2019.

[35] C. Zhang, G. Gholipour, and A. A. Mousavi, "Nonlinear dynamic behavior of simply-supported RC beams subjected to combined impact-blast loading," *Engineering Structures*, vol. 181, pp. 124–142, 2019.

[36] C. Zhang and H. Wang, "Robustness of the active rotary inertia driver system for structural swing vibration control subjected to multi-type hazard excitations," *Applied Sciences*, vol. 9, no. 20, pp. 16–32, 2019.

[37] S. Chen, Y. Song, L. Kong et al., "Study on approach to identification and classification of expansive soils," *Rock and Soil Mechanics*, vol. 26, no. 12, pp. 1895–1900, 2005.

[38] Li Sun, C. Li, C. Zhang et al., "Early monitoring of rebar corrosion evolution based on FBG sensor," *International Journal of Structural Stability and Dynamics*, vol. 18, no. 8, pp. 11–22, 2018.

[39] A. A. Mousavi, C. Zhang, S. F. Masri, and G. Gholipour, "Structural damage localization and quantification based on a CEEMDAN hilbert transform neural network approach: a model steel truss bridge case study," *Sensors*, vol. 20, no. 5, pp. 1271–1294, 2020.

[40] M. Abedini, C. Zhang, J. Mehrmashhadi, and E. Akhlaghi, "Comparison of ALE, LBE and pressure time history methods to evaluate extreme loading effects in RC column," *Structures*, vol. 28, pp. 456–466, 2020.

[41] J. Zheng, C. Zhang, and A. Li, "Experimental investigation on the mechanical properties of curved metallic plate dampers," *Applied Sciences*, vol. 10, no. 1, pp. 269–284, 2020.

[42] G. Gholamreza, C. Zhang, and M. Asma Alsadat, "Numerical analysis of axially loaded RC columns subjected to the combination of impact and blast loads," *Engineering Structures*, vol. 219, pp. 110924–110949, 2020.

[43] Li Sun, Z. Yang, Q. Jin et al., "Effect of axial compression ratio on seismic behavior of GFRP reinforced concrete columns," *International Journal of Structural Stability and Dynamics*, vol. 20, no. 6, pp. 16–31, 2020.

[44] M. Abedini and C. Zhang, "Dynamic performance of concrete columns retrofitted with FRP using segment pressure technique," *Composite Structures*, vol. 260, Article ID 113473, 2021.

[45] W. Zhang, Z. Tang, Y. Yang et al., "Assessment of FRP–concrete interfacial debonding with coupled mixed-mode cohesive zone model," *Journal of Composites for Construction*, vol. 25, no. 2, 2021.

[46] GB/T5012-1999, *Geotechnical Test Method Standard*, ASTM International, West Conshohocken, PA USA, 1999.

[47] Y. Bai, S. Wang, B. Mou et al., "Bi-directional seismic behavior of steel beam-column connections with outer annular stiffener," *Engineering Structures*, vol. 227, pp. 16–41, 2021.

[48] J. Zhu, K. Yang, Y. Chen et al., "Revealing the substitution preference of zinc in ordinary Portland cement clinker phases: a study from experiments and DFT calculations," *Journal of Hazardous Materials*, vol. 409, pp. 124504–124514, 2021.

[49] F. Chen, Z. Jin, E. Wang et al., "Relationship model between surface strain of concrete and expansion force of reinforcement rust," *Scientific Reports*, vol. 11, no. 1, pp. 4208–4231, 2021.

[50] J. Zhu, Y. Chen, L. Zhang et al., "Revealing the doping mechanism of barium in sulfoaluminate cement clinker phases," *Journal of Cleaner Production*, vol. 295, Article ID 126405, 2021.

[51] M. Hongyan, "Mercury intrusion porosimetry in concrete technology: tips in measurement, pore structure parameter acquisition and application," *Journal of Porous Materials*, vol. 21, no. 2, pp. 207–215, 2014.

[52] R. Vocka, C. Galle, and M. Dubois, "Mercury intrusion porosimetry and hierarchical structure of cement pastes: theory and experiment," *Cement and Concrete Research*, vol. 30, no. 4, pp. 521–527, 2000.

[53] H. Huang, M. Guo, W. Zhang et al., "Numerical investigation on the bearing capacity of RC columns strengthened by HPFL-BSP under combined loadings," *Journal of Building Engineering*, vol. 39, Article ID 102266, 2021.

[54] K. Zhang, J. Zhang, X. Ma et al., "History matching of naturally fractured reservoirs using a deep sparse autoencoder," *SPE Journal*, pp. 1–22, 2021.

[55] W. C. Fontes, J. M. Franco de Carvalho, L. C. Andrade, A. M. Segadães, and R. A. F. Peixoto, "Assessment of the use potential of iron ore tailings in the manufacture of ceramic tiles: from tailings-dams to "brown porcelain," *Construction and Building Materials*, vol. 206, pp. 111–121, 2019.

[56] Z. Tian, Z. Zhao, and C. Dai, "Experimental study on the properties of concrete mixed with iron ore tailings," *Advances in Materials Science and Engineering*, vol. 2016, Article ID 8606505, 9 pages, 2016.

[57] S. Pul, "Experimental determination of cohesion and internal friction angle on conventional concretes," *ACI Materials Journal*, vol. 114, no. 3, pp. 407–415, 2017.

[58] M. Hattab, T. Hammad, and J.-M. Fleureau, "Internal friction angle variation in a kaolin/montmorillonite clay mix and microstructural identification," *Géotechnique*, vol. 65, no. 1, pp. 1–11, 2015.

[59] Y. Hu, S. Wu, J. Withers Philip et al., "Corrosion fatigue lifetime assessment of high-speed railway axle EA4T steel with artificial scratch," *Engineering Fracture Mechanics*, vol. 245, Article ID 107588, 2021.

[60] D. L. Shear, H. W. Olsen, and K. R. Nelson, *Effects of Desiccation on the Hydraulic Conductivity versus Void Ratio Relationship for a Natural Clay*, Transportation Research Board, New York, NY, USA, 1992.